

Nature of the many-particle potential in the monatomic liquid state: Radial and angular structure

B. E. Clements and D. C. Wallace

Theoretical Division, Los Alamos National Laboratory, Los Alamos, New Mexico 87545

(Received 15 September 1998)

The atomic configurational order of random, symmetric, and crystalline states of sodium is investigated using molecular-dynamics simulations. Pair distribution functions are calculated for these states. Consistent with the liquid- and random-state energetics, we find that, by cooling, the liquid configurations evolve continuously to random-state structures. For sodium, the random pair distribution function has a split second peak characteristic of many amorphous materials and has the first subpeak exceeding the second subpeak. Experiments have shown this to be the case for amorphous Ni, Co, Cr, Fe, and Mn. A universal pair distribution function is identified for all random structures, as was hypothesized by liquid-dynamics theory. The peak widths of the random pair distribution function are considerably broader, even at very low temperatures, than those of the bcc and symmetric structures. No universal pair distribution function exists for symmetric structures. For low-temperature random, symmetric, and crystalline structures we determine average Voronoi coordination numbers, angular distributions between neighboring atomic triplets, and the number of Voronoi edges per face. Without exception the random and symmetric structures show very different trends for each of these properties. The universal nature of the random structures is also apparent in each property exhibited in the Voronoi polyhedra, unlike for the symmetric structures. Angles between neighboring Voronoi triplets common to random close-packing structures are favored by the random structures whereas those hinting at microcrystalline order are found for the symmetric structures. The distribution of Voronoi coordination numbers for both random and symmetric structures are peaked at 14 neighbors, but while the symmetric structures are essentially all 14, the random structures have nearly as many 13 and 15 neighbor polyhedra. The number of edges per face also shows a stark difference between the random and symmetric structures; the number is broadly distributed about the peak value 5 for the random structures, but contains many more four- and six-edged faces (and very few five-edged faces) for the symmetric structures. [S1063-651X(99)02203-5]

PACS number(s): 61.20.Ne, 61.20.Ja, 61.20.Gy

I. INTRODUCTION

In liquid dynamics theory [1] we postulated the existence of a very large number of nearly harmonic valleys in the many-particle potential surface. The stable equilibrium configuration at the bottom of a many-particle valley was called a structure. Noncrystalline or amorphous structures have long been observed in molecular-dynamics (MD) calculations [2–6]. An important step in liquid-dynamics theory was to divide the amorphous structures into two classes, random and symmetric. The symmetric structures are supposed to have a remnant of crystal symmetry among near neighbors, and because of this symmetry, are expected to be relatively few in number, and to have a significant spread in their macroscopic properties. The random structures are supposed to have near-neighbor arrangements as random as possible (compatible with the interatomic potential), and because of this randomness, are expected to be overwhelmingly most numerous, and to be macroscopically uniform. This classification is useful in liquid-dynamics theory, since it allows one to ignore the more complicated but statistically insignificant symmetric structures, and to write a partition function as a sum over a large number of equivalent random structure valleys. In the preceding paper, we used MD calculations to study a classical system of particles interacting through the metallic sodium potential, at the fixed density of liquid sodium at melt [7]. We indeed found two distinct groups of

many-particle structures. The energetically higher-lying group was called random, since they are overwhelmingly most numerous and macroscopically uniform, and the lower-lying group was called symmetric, since they are few in number and not macroscopically uniform. It still remains to examine the symmetry properties of these structures, i.e., to examine the geometry of the arrangements of the particles in configuration space to see if the random and symmetric properties are present as expected. This examination is the objective of the present work. In the end we shall find several new results regarding the geometric characterization of random and symmetric structures, and on the thermal broadening of the pair correlations for temperatures up to and including liquid states.

In Sec. II, we investigate the radial correlations in atomic configuration space by using our MD-calculated pair distribution function $g(r)$. We do this for the bcc crystal, and for random and symmetric states. We note that a considerable portion of the work in Refs. [2–6] was devoted to examining the radial and angular configurational order in low-temperature liquid and amorphous solid states. Because the concept of random and symmetric states had not been established, no attempt was made to categorize their findings accordingly. In contrast, here special importance is placed on comparing and contrasting the $g(r)$'s for the different classes of states: random, symmetric, and crystalline. Our findings demonstrate that the nature of the configurational order is

strongly dependent on the class to which the many-particle valley belongs.

To deepen our understanding of the configurational order it becomes necessary to identify a length scale akin to a nearest-neighbor distance R_{nn} . One popular (though arbitrary) choice is take R_{nn} as the point where $g(r)$ acquires a minimum value between its first and second maxima. Because of the limitations of that approach, we have chosen to proceed differently by constructing the well-known Voronoi polyhedra specific to each atom (Sec. III). The Voronoi polyhedra provide a partitioning of space into N subvolumes, such that the space contained in a given polyhedron is associated with one and only one atom. The Voronoi construction is *unique* and fills all of space. The advantage of this construction is that the number of faces, the number of edges per face, and so on, all provide information on the local configurational order. We use the Voronoi construction to determine average Voronoi coordination numbers (Sec. III A), angular distributions between neighboring atomic triplets (Sec. III B), and the number of Voronoi edges per face (Sec. III C) for the random and symmetric classes.

The pair distribution functions for the random structures show a strong similarity to those that have been measured for several transition metals that have been arrested in amorphous states. In Sec. IV we review several such experiments and make connections to the present work. Closing statements in Sec. V briefly summarize our work.

II. PAIR DISTRIBUTIONS AT ALL TEMPERATURES

The pair distribution function $g(r)$, for liquids, crystals, and amorphous materials, contains useful information about the interparticle radial correlations. Our MD pair distribution functions are calculated in the standard way. About each particle, concentric radial bins are constructed with a chosen small bin width Δr , with the proviso that Δr is sufficiently small to resolve numerically all relevant structure in $g(r)$. The number of neighbors $n(r)$ (a neighbor may be the periodic image particle) for each particle is counted in each bin. The ensemble average (time average for an MD equilibrium state) of $n(r)$ is then taken. Using the standard normalization factor that makes $g(r)$ tend to unity as the correlations tend to zero, $g(r)$ is expressed as

$$g(r) = \frac{V}{4\pi N r^2 \Delta r} \langle n(r) \rangle, \quad (2.1)$$

where N is the particle number, V is the system volume, and the brackets indicate the time average plus the average over all particles. Periodic boundary conditions are invoked in our MD simulations.

One of the important findings of Ref. [7] is that, for monatomic supercooled sodium, there exist temperatures in the range of $35 \text{ K} \lesssim T \lesssim 200 \text{ K}$, where transitions from the random to the symmetric branch occur readily during the action of running pure MD (Sec. II B of Ref. [7]). Even in those situations one can still calculate meaningful “equilibrium” $g(r)$. This is because of the relatively high temperatures spanned by the transition window, and because it is always readily possible to find potential and kinetic energy plateaus that are (meta)stable and persist for many thousands of MD

iterations. Parenthetically, the minimal acceptable number of stable iterations was taken by us to be 2000, but it was not uncommon to find stable plateaus that persisted for on the order of 150 000 MD iterations. When calculating $g(r)$, only those MD iterations were included in the time average where the system remained on the flat portion of the potential energy plateau. In this way, the reported $g(r)$ are specific to either states on the random branch or the symmetric branch and were never averaged over a mixture of random and symmetric states, nor the transition region separating them.

Before proceeding with our discussion on the state dependence of the pair distribution function, we first introduce several variants of $g(r)$ that are useful in our analysis. When the system is localized within a single many-particle valley, as we observed for low temperatures, we shall denote the associated pair distribution function by $g_\gamma(r)$. The index γ is the valley label. We also define the *structure* pair distribution function $G_\gamma(r)$, for valley γ , in the limit that the system becomes frozen into a structure.

The bcc crystal will provide us with an important reference state since considerable information is already known about the nature of the bcc pair correlations. In Sec. II A, it provides us with a reference pair distribution function to compare to those of the random and symmetric $g_\gamma(r)$'s. Consequently, we will begin our discussion with the temperature dependence of bcc $g(r)$, obtained from MD using the sodium potential of Ref. [7]. This is followed by discussions on the random (II B) and symmetric (II C) state pair distribution functions.

A. bcc states

Choose $r=0$ to be an occupied bcc lattice site, then as the temperature is decreased to zero, $n(r)$ in Eq. (2.1) converges to a value (perhaps zero) equal to the number of lattice sites in the spherical shell of radius r and bin width Δr , centered about the point $r=0$. Omitting quantum effects, at $T=0$, in the limit of $\Delta r \rightarrow 0$, the bcc pair distribution function $g_\gamma(r)$ becomes the sum of a set of true δ functions. This defines the *structure* distribution function $G_\gamma(r)$. Since it is unique ($\gamma=1$) we will denote it by $G_{\text{bcc}}(r)$.

At any finite temperature, the δ functions of $G_{\text{bcc}}(r)$ thermally broaden and the bcc pair distribution function is properly referred to as $g_{\text{bcc}}(r)$. Since the characteristic measures of the potential energy curvature of the bcc valley (Θ_0 , Θ_2 , and Θ_{-2}) are approximately the same as those of the random and symmetric valleys [7], then at any given temperature, the width of the peaks in $g_{\text{bcc}}(r)$ will give an estimate of the thermal broadening present in the random and symmetric valley $g_\gamma(r)$'s at the same temperature.

In Fig. 1, three different-temperature MD $g_{\text{bcc}}(r)$ are shown. Here, $N=432$ since this number of atoms in a bcc arrangement packs perfectly in a cubical box with periodic boundary conditions. Note, even as low as $T=0.356 \text{ K}$, $g_{\text{bcc}}(r)$, while having extremely narrow peaks, is nevertheless not converged to G_{bcc} . By further reducing the temperature the peak heights continue to grow while their widths continue to decrease. At $T=0$, when every atom is resting at its minimum in potential, true δ functions will be realized and $g_{\text{bcc}}(r)$ converges to $G_{\text{bcc}}(r)$. The effects of thermal

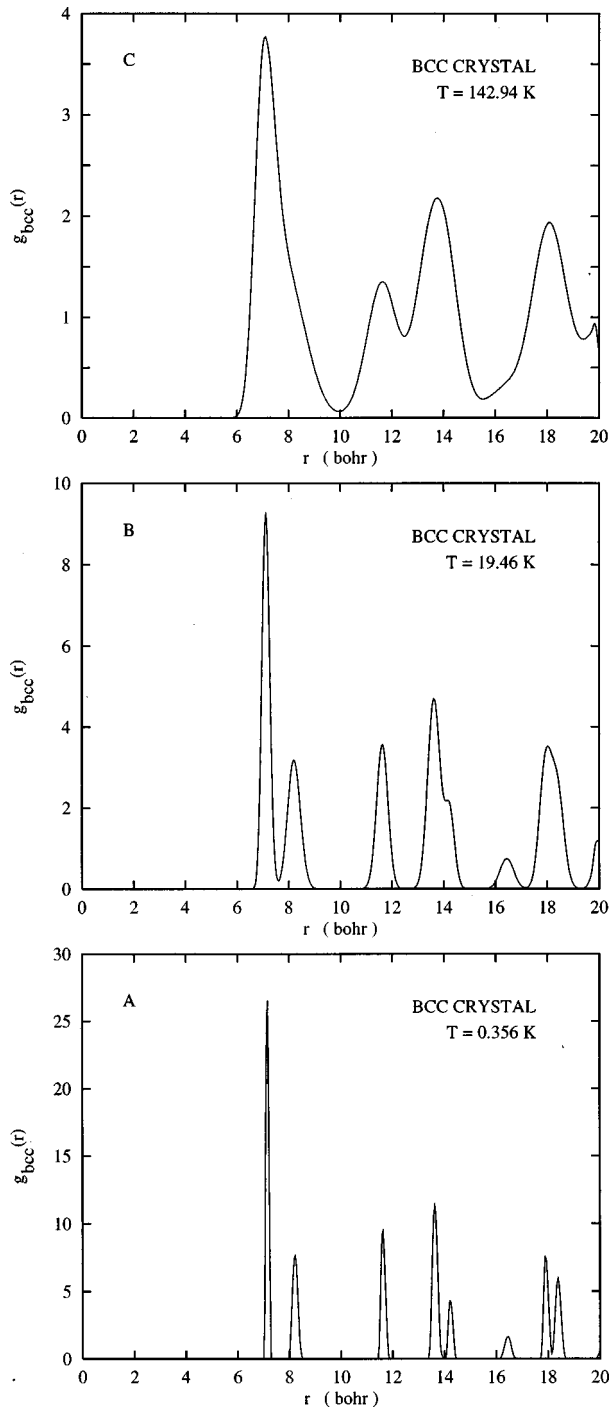


FIG. 1. The bcc pair distribution function $g_{\text{bcc}}(r)$ for three different temperatures.

broadening, with increasing temperature, are clearly evident in this figure. We also draw the readers attention to the double split-peak structure on the the second maximum of $g_{\text{bcc}}(r)$ at $T=142.94$ K, the details of which will be discussed in Sec. II B and then again in Sec. IV. Results similar to those in Fig. 1(c) have been reported by Brown and Mountain [8] for supercooled liquid Rb.

B. Random states

In this subsection we establish two important properties of the random pair distribution functions. The first property is

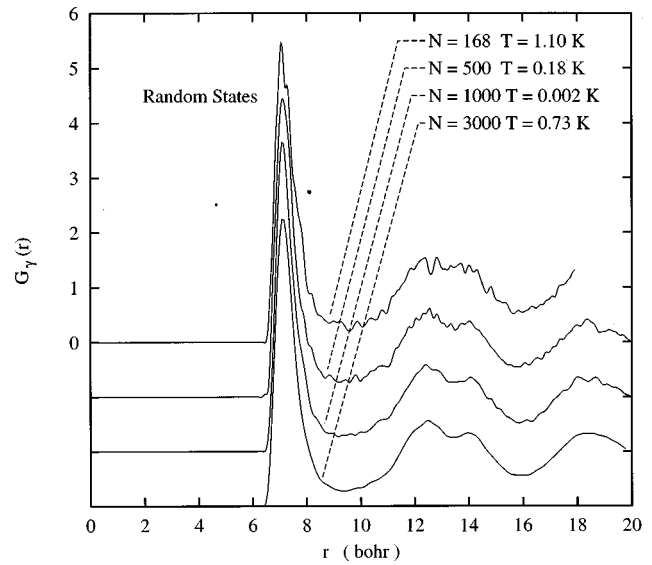


FIG. 2. Random structural pair distribution function $G_{\gamma}(r)$ for four different random valleys. The small wiggles on these curves vanish as N increases.

the *universal* nature of the r dependence of $G_{\gamma}(r)$ for random structures. The second property pertains to the continuous evolution of $g(r)$ from the liquid to the random states as the temperature is reduced into the supercooled regime. This second property provides further evidence linking the liquid and random states.

To expound on the first property, we use our MD simulations to calculate the pair distribution function for low temperature ($T \leq 3$ K) random states. The pair distribution functions for four different random valleys are shown in Fig. 2. The potential and kinetic energies for these four valleys are consistent with energies on the random branch (Fig. 3 of Ref. [7]), and the system is no longer sampling multiple random valleys (see Fig. 11 of Ref. [7]), at least for time

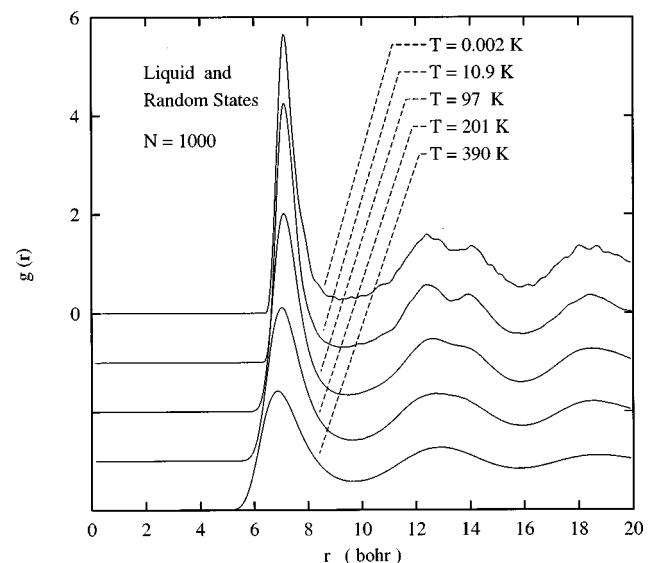


FIG. 3. The liquid pair distribution function ($T=390$ K) and random pair distribution functions ($0.002 \text{ K} \leq T \leq 201 \text{ K}$). This figure illustrates the continuous evolution of the random states into the liquid, with increasing temperature.

durations relevant in our simulation.

The four $g_\gamma(r)$ are very similar to one another with the exception of small wiggles that are increasingly pronounced with decreasing N . When overlaid, one on top of the other, the four $g_\gamma(r)$ differ *only* by these wiggles. The wiggles are N dependent, and appear to be absent by $N=3000$. The origin of the wiggles is clear and will be elaborated on at the end of this subsection.

By reducing the temperature of the $N=3000$ valley below 0.73 K we find essentially no quantitative change in the shape of $g_\gamma(r)$. This is also true for the other three random valleys. We conclude that the $N=3000$ pair distribution function has converged to the *structure* pair distribution function $G_\gamma(r)$, associated with its valley γ . If we ignore, as we should, the wiggles that arose from finite-size effects, the other three valleys have converged to the same $G_\gamma(r)$. Moreover, our investigation, through numerous quenches into the random valleys, has demonstrated with overwhelming evidence, that a single *universal* $G_\gamma(r)$ exists (omitting the small N wiggles), which we call $G_{\text{Ran}}(r)$. This observation is in agreement with the prediction of liquid dynamics theory, that random valleys have universal average properties in the large N limit. [1]

We now turn to the second property of the random $g_\gamma(r)$. The random valleys possess order that is much more liquid-like than (micro)crystallinelike, thus it is obvious that one should study the temperature evolution of these states with the goal of relating the liquid to the random states.

From very low temperatures, for example, 10^{-3} K, up to near 3 K, $g_\gamma(r)$ is independent of temperature. As just discussed, this constant low- T function is an expression of $G_\gamma(r)$. Thermal effects become readily noticeable above 10 K. For example, the height of the first peak, which is approximately 5.3 for temperatures up to 10 K, drops to approximately 5 at 25 K. Figure 3 shows the continuous evolution of the pair distribution function for the random states up to normal liquid temperatures. It is evident from this figure that liquid states are properly viewed as a subset of the random states. This is of course consistent with the notion that the liquid and random states fall on a single branch in kinetic energy versus potential energy space.

We now focus on several miscellaneous, *albeit* relevant topics regarding $g_{\text{Ran}}(r)$.

(i) The random structure $G_{\text{Ran}}(r)$ has first, second, third, and so forth, maxima. Inspection of Fig. 2 shows that the second maximum (centered at approximately $13a_0$) is split into a first and a second subpeak, and moreover, the first subpeak exceeds the strength of the second subpeak. When compared to the counterexamples (Secs. II A and II C), this behavior of the split-peak strength is characteristic *alone* of the random states. For the bcc case, the broad peak at the same location in $g_{\text{bcc}}(r)$ [Fig. 1(c)], which comprises the third- and the fourth-neighbor shells, is also split, but with the first subpeak *lower* than the second. We shall return to this point in Sec. II C and then again in Sec. V.

(ii) The maxima widths exhibited by $G_{\text{Ran}}(r)$ are in sharp contrast to those of $g_{\text{bcc}}(r)$. $G_{\text{Ran}}(r)$ has a very broad first neighbor maximum, relative to the crystal (and also to the symmetric states discussed in Sec. II C). For example, the first maximum of $G_{\text{Ran}}(r)$ has a width comparable to that of the first maximum of $g(r)$ for a bcc crystal at a temperature

near 150 K. The increased width of the maxima of $G_{\text{Ran}}(r)$ are caused by the random placement of atoms, and not by thermal vibrations of atoms about their equilibrium positions.

(iii) In this work we are often in regimes of extreme low temperatures where quantum effects should not be negligible. The role of quantum effects will be to further broaden and smooth the pair distribution functions. We refer the reader to Campbell's review [9] for a comprehensive discussion on pair distribution functions in quantum liquids.

(iv) We now return to finite-size effects, discussed above, that led to the small wiggles observed in Fig. 2. Relative to $r=0$, each random $g_\gamma(r)$ can be decomposed into a set of thermally broadened δ functions. One expects the thermal-broadened width of each δ function to be on the order of those in Fig. 1(a), for the bcc crystal. [Note, the widths of the wiggles for $N=168$ in Fig. 2 appear consistent with the δ function widths of Fig. 1(a).] For $N=168$, the δ functions are few enough in number such that, even upon averaging over all N particles, they can still be resolved from the background distribution. However, for $N=3000$, this is no longer the case, and the number of δ functions is so great that they are no longer discernible. As N tends to infinity, we believe the distribution function will remain smooth even at zero temperature and as $\Delta r \rightarrow 0$. Of course, in any real system, quantum effects will additionally smooth $G_{\text{Ran}}(r)$.

C. Symmetric states

We now compare and contrast $g(r)$ for symmetric states with the bcc and random ones. The overall conclusion is that $g(r)$ for any symmetric state is clearly distinguishable from $g(r)$ for *any* crystal, and from the $g_{\text{Ran}}(r)$. We will further demonstrate that $G_\gamma(r)$ for any symmetric valley γ is typically different for each symmetric valley. Consequently, *no* universal $G_{\text{Sym}}(r)$ exists. We now summarize our findings.

First, for each symmetric valley, $g_\gamma(r)$ loses temperature dependence and converges to a constant curve as the temperature is lowered. Specifically, $g_\gamma(r)$ changes very little below 10 K, and changes almost imperceptibly below 1 K. Hence, at these low temperatures $g_\gamma(r)$ has seemingly converged to the structure pair distribution function $G_\gamma(r)$. $G_\gamma(r)$'s for three different symmetric structures are shown in Fig. 4. While this low-temperature convergence property is essentially the same for symmetric and random valleys, it distinguishes a symmetric valley from any crystalline valley.

Second, for a symmetric valley, $G_\gamma(r)$ is highly irregular in the sense that it is composed of a significant number of narrow peaks (c.f. Fig. 4), the number being 50% more than for the bcc lattice, out to $20a_0$. This composition implies that the symmetric structure has more symmetry than the random structure but less than the bcc crystal.

Third, the locations and magnitudes of the peaks in $G_\gamma(r)$ differ noticeably from one symmetric valley to another (Fig. 4). This agrees with the prediction of liquid-dynamics theory [1] that symmetric structures possess a wide variation in their average properties, even in the large N limit. Above a temperature of around 100 K the subpeaks have broadened to the point where $g_\gamma(r)$ is a rather smooth function of radial

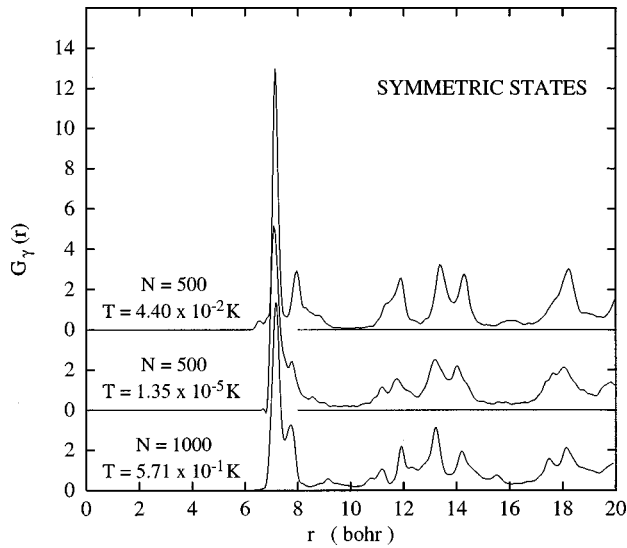


FIG. 4. Three low-temperature $G_\gamma(r)$ for three different symmetric structures.

position r . Figure 5 shows three examples of $g(r)$ for states on the symmetric branch.

Fourth, two more noteworthy features distinguish any symmetric $G_\gamma(r)$ from the universal $G_{\text{Ran}}(r)$. First, the first-neighbor maximum of $G_\gamma(r)$ is narrower than $G_{\text{Ran}}(r)$; it is approximately twice as high and half as wide. Second, in $G_\gamma(r)$, the broad maximum at $r \approx 11-15a_0$ gets resolved into four to five peaks (Fig. 4). As demonstrated in Fig. 5, when smoothed by thermal broadening at $T \geq 100$ K, this becomes a broad split maximum, with the first subpeak *lower* in height than the second, like the bcc structure but opposite to $g_\gamma(r)$ for a random valley. In this work, we observed that all $g(r)$'s from the symmetric branch had this characteristic behavior for their second maxima, indicating a possible universal property of the elevated-temperature symmetric $g(r)$'s.

III. VORONOI DISTRIBUTIONS AT ZERO TEMPERATURE

We will now make a more detailed study of the configurational arrangements among near neighbors in random and symmetric structures. This is conveniently done in terms of the Voronoi polyhedra. For a given configuration of the particles, the Voronoi polyhedron for each particle is unique. To construct it draw lines connecting this particle with all other particles, bisect each line with a normal plane, and take the smallest polyhedron enclosing the original particle. For any configuration, the Voronoi polyhedra fill space, and each face belongs to two polyhedra. If the configuration of the particle is a crystal lattice, the Voronoi polyhedra are the Wigner-Seitz cells. When the meaning is clear, we use the simple term ‘‘polyhedra.’’

At zero temperature, the particles are located at the minimum of a valley in the many-particle potential surface. This stable equilibrium configuration is a structure, and we are interested in local geometry of structures, as measured, for example, by the number of near neighbors, or the angles formed by near-neighbor triplets. If the system is warmed from zero temperature, these measures of local geometry will

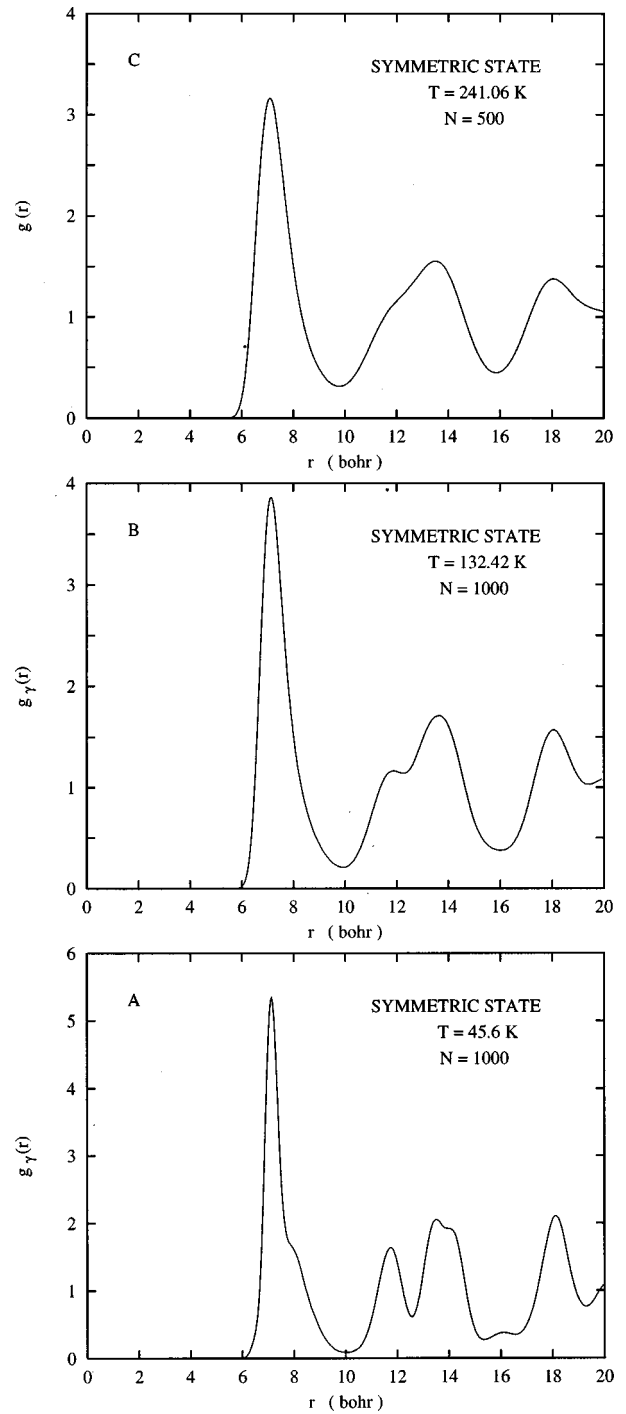


FIG. 5. Temperature dependence of the symmetric state $g(r)$. In (a) and (b) the system is confined to a single symmetric valley, while in (c) the system exhibits a slow diffusion among symmetric valleys.

become broadened by the thermal motion of the particles. Such broadening merely obscures the underlying structural geometry, and so we eliminate it by working only with MD systems at very low temperatures, at $T \leq 10^{-3}$ K, where our data accurately represents the condition $T = 0$.

A. Distribution of coordination numbers

The number of faces of a polyhedron is a coordination number, but is not simply the number of nearest neighbors.

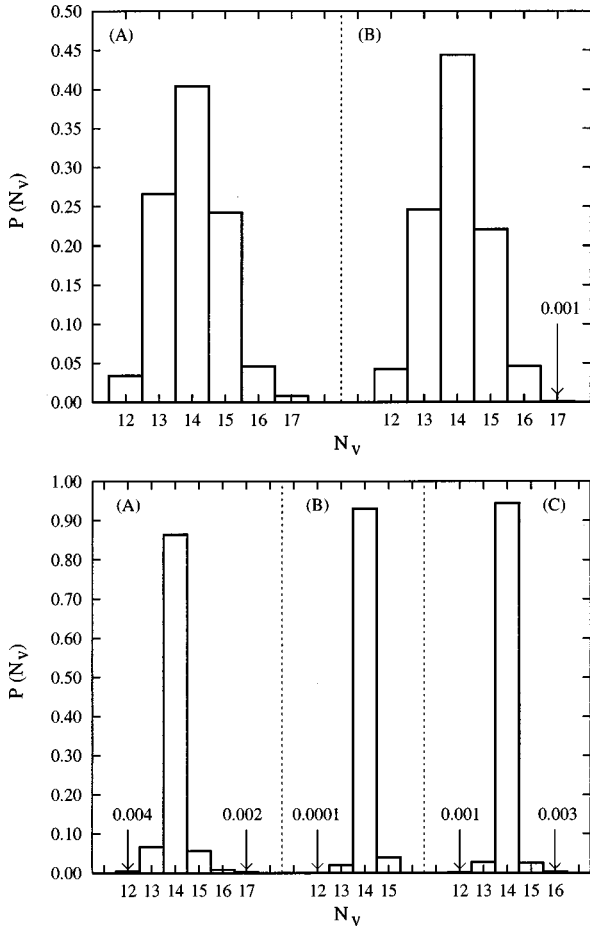


FIG. 6. Distribution $P(N_v)$ of the Voronoi coordination numbers N_v for two different random structures (top) and three different symmetric structures (bottom).

To see this, consider the primitive cubic lattices of bcc and fcc structures. For the bcc crystal, the polyhedron has eight hexagonal faces that bisect lines from the central particle to its eight nearest neighbors, and has six square faces that bisect lines from the central particle to its six second neighbors. Hence for the bcc crystal, the polyhedron has 14 faces, and the 14 coordinated particles constitute both nearest- and next-nearest neighbors. For an fcc crystal, the polyhedron has 12 rhombic faces that bisect lines from the central particle to its 12 nearest neighbors, and that is all. However, for the fcc crystal, lines from the central particle to its six second neighbors pass through the vertices where four faces meet, at half the distance to the second neighbors. If, for example, two of the fcc second neighbors are each moved a little closer to the central particle, then the two vertices of the polyhedron will become small planes, and the number of faces will be 14. For the random and symmetric structures we find here, the polyhedra have from 12 to 17 faces. For a given central particle, the number of its polyhedron faces is called its coordination number, denoted by N_v , and the coordinated neighbors are called its Voronoi neighbors.

Figure 6 shows the normalized distribution of coordination numbers $P(N_v)$ for two random structures and for three symmetric structures. The universal property of these graphs is that $N_v=14$ is the most prevalent value. Beyond this, the

distribution for random and symmetric structures are in stark contrast. The random distribution is rather broad, with contributions from $N_v=13$ and 15 being at least half the contribution from $N_v=14$, and with significant contributions also from $N_v=12$ and 16 . The symmetric distribution is very narrow, being almost entirely $N_v=14$, only very small contributions from $N_v=13$ and 15 , and nothing else of importance. The distributions $P(N_v)$ we have found are qualitatively the same for all random structures on the one hand, and qualitatively the same for all symmetric structures on the other hand. As is clear from Fig. 6, given the graph of $P(N_v)$ for any noncrystalline structure found in the present study, we can positively identify the structure as random or symmetric.

B. Angles between Voronoi neighbor pairs

The lines from the central particle to two of its Voronoi neighbors intersect at angle θ . The distribution of these angles, normalized so that it is a probability density, is denoted $P(\theta)$. Here the normalization is made in terms of θ in degrees:

$$\int_0^{180} P(\theta) d\theta = 1. \quad (3.1)$$

Obviously, for a given polyhedron, the set of angles will exhibit some dependence on the number of faces, since at the very least, the more the faces present, the smaller the angles will tend to be. It is therefore of interest to classify the polyhedra according to their number of faces, and to evaluate $P(\theta)$ separately for each class.

Figure 7 shows a set of five $P(\theta)$ distributions for random structures, and each $P(\theta)$ representing polyhedra with fixed N_v , for $N_v=12-16$. Each graph shows $P(\theta)$ for two different random structures, one each with 500 and 1000 particles. We notice that the two distributions in each graph are essentially identical, differing only in their fluctuations. Hence Fig. 7 demonstrates once again that different random valleys are macroscopically identical up to fluctuations, or equivalently, are macroscopically identical in the limit $N \rightarrow \infty$. The larger fluctuations at $N_v=12$ and 16 result from having fewer samples of polyhedra with these coordination numbers.

The general characteristics of $P(\theta)$ for the random structures, as seen in Fig. 7, are a broad distribution, with peaks around 60 and 120 , and with movement toward smaller angles as N_v increases. For the peak at 60 , rather symmetric in shape at $N_v=12$, a small shoulder at smaller angle, say, approximately 50 , appears at $N_v=13$, and this shoulder grows and moves to still smaller angles as N_v increases, until at $N_v=16$ the whole feature becomes a band in the range $40-60$. Again, starting at $N_v=12$, where broad peaks are present at approximately 120 and 170 , a similar development through the appearance and growth of new shoulders moves these peaks, respectively, to approximately 100 and 145 at $N_v=16$.

Figure 8 shows a set of three $P(\theta)$ distributions, corresponding to $N_v=13, 14$, and 15 for a single symmetric structure. Again, the larger fluctuations at $N_v=13$ and 15 result

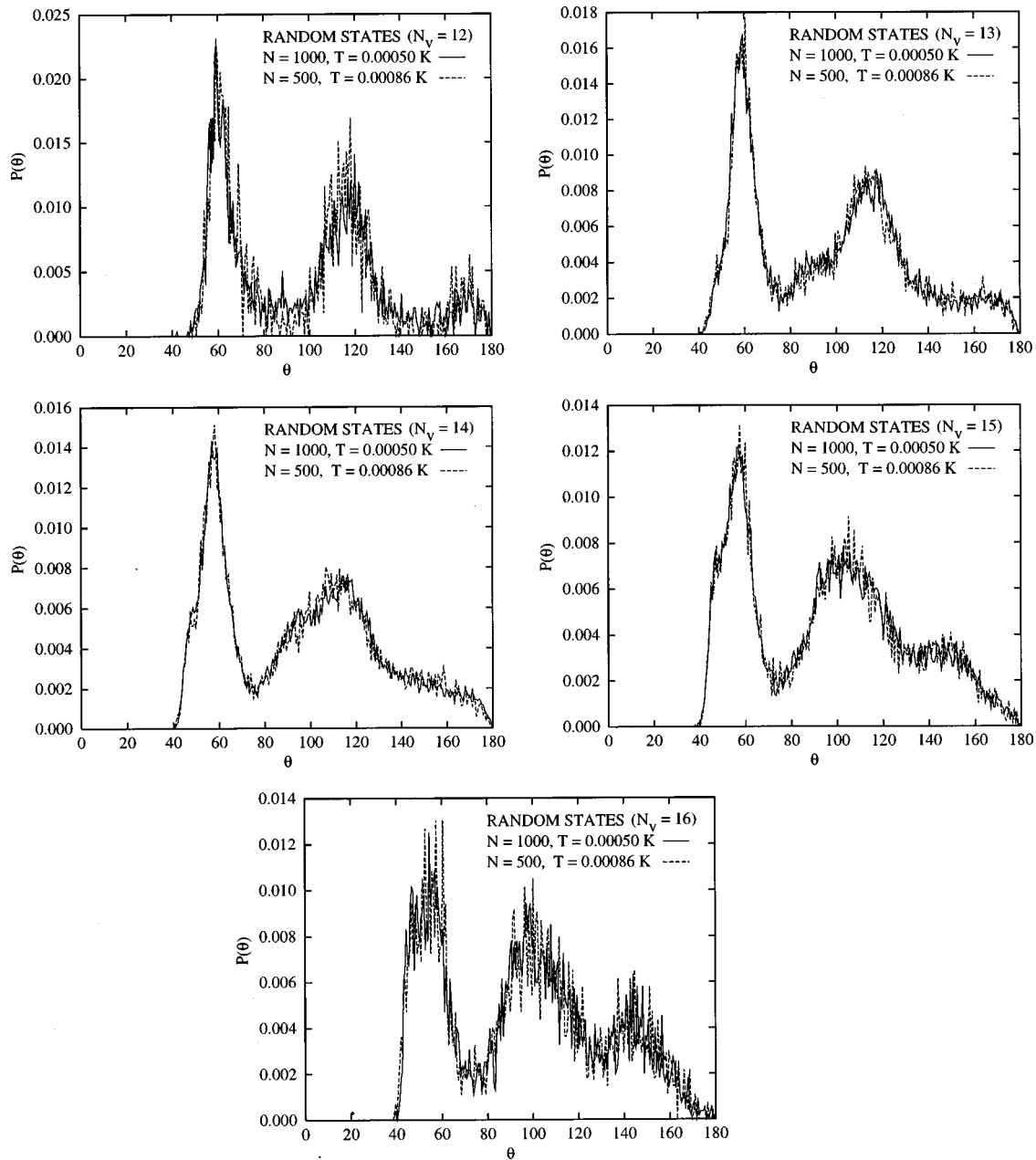


FIG. 7. Distribution of angular correlations $P(\theta)$ between Voronoi neighbors for two different random structures (θ in degrees).

from having fewer samples of polyhedra with these coordination numbers. At $N_v = 13$, $P(\theta)$ has major peaks at 60, 90, 120, and 180. Upon increasing N_v to 14, new peaks appear above 60 and below 120, at approximately 65 and 115, respectively. But then, upon increasing N_v to 15, those two peaks recede, and others appear below 60 and above 120, at approximately 45 and 135, respectively. Through this evolution, the peaks at 60, 90, 120, and 180 remain intact.

In the symmetric graphs of Fig. 8, the narrowness of the peaks, and their appearance and disappearance with changing N_v , suggests that the structure is composed of a set of local clusters of different symmetries, and with significant range of angular distortions among clusters. We may notice that the angles 60, 90, 120, and 180 appear among nearest neighbors for fcc; 90 and 180 appear among nearest and next-

nearest neighbors for bcc; 45 and 135 appear among nearest and next-nearest neighbors for fcc; while 65 and 115 do not appear among nearest and next-nearest neighbors for either fcc or bcc. However, the symmetric $P(\theta)$ in Fig. 8 represents $T=0$, while the $T=0$ distribution for a crystal structure is a set of δ functions, so clearly, any local bcc crystalline symmetry that might be present is strongly distorted in the symmetric structure.

It was shown in the last section, by comparison of the pair distribution functions, that the symmetric structures are noticeably different from one another (see Fig. 4). We can see this again in Fig. 9, which shows $P(\theta)$ at $N_v = 14$ for three different symmetric structures. The three $P(\theta)$ are qualitatively similar, with all showing the same main peaks at around 60, 90, 120, and 180, but the three exhibit quantita-

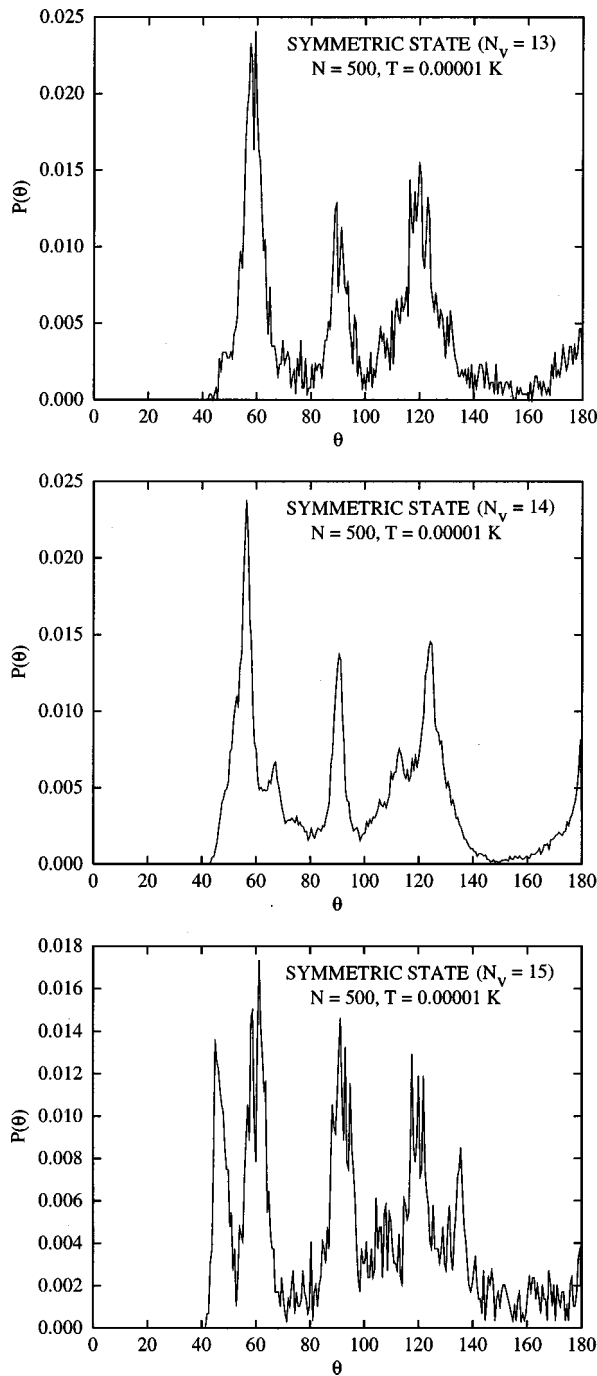


FIG. 8. Distribution of angular correlations $P(\theta)$ between Voronoi neighbors for a symmetric structure (θ in degrees).

tive differences that are well outside the fluctuations. These differences are a notable property of symmetric structures, and apparently survive as $N \rightarrow \infty$.

Compared to the random $P(\theta)$ distributions, the symmetric $P(\theta)$ are sharper and more detailed, that is, they exhibit more and narrower peaks. In addition, the prominent sharp peak at 90 in the symmetric structure, and the weaker peak at 180, are never seen in the random structure. In the present work, the general sharpness of $P(\theta)$ is sufficient to distinguish the symmetric structures from the random structure. Given a single graph of $P(\theta)$, for any N_v shown for random structures in Fig. 7, or for any N_v shown for a symmetric

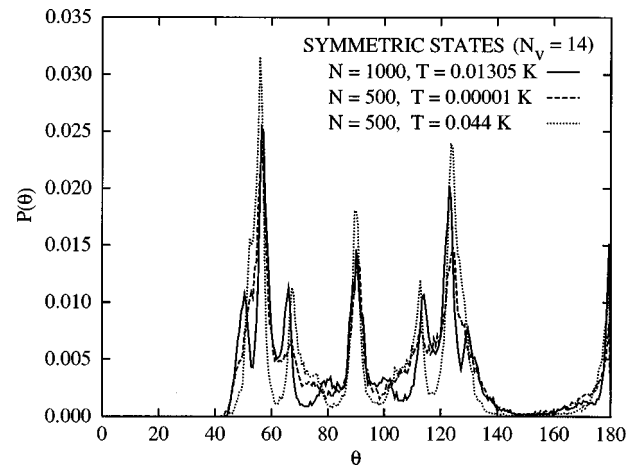


FIG. 9. Over-laid distributions of angular correlations $P(\theta)$ between Voronoi neighbors for three different symmetric structures (θ in degrees).

structure in Fig. 8, we can positively identify the structure as random or symmetric.

C. Number of edges per face

The number of edges per face proves a most interesting statistical measure. This measure is presented in Fig. 10, in the form of a bar graph of the number of faces which have 3, 4, \dots , 7 edges. Graphs are shown for a random structure, and a symmetric structure, each with 1000 particles. Again, the data are shown separately for polyhedra with 12–16 faces. The normalization is such that the total number of faces in each separate bar graph, labeled by N_v , is the total number of faces in the set of polyhedra with N_v faces, for the structure in question. The one exception is the symmetric graph for $N_v = 14$, which was reduced by a factor of 20, to scale away the approximately 20-fold majority of $N_v = 14$ polyhedra in the symmetric structure (see Fig. 6).

The universal properties we have found, for both random and symmetric structures, are the number of edges runs from 3 to 9, while most faces have four, five or six edges. Here the similarity ends, and a stark difference between random and symmetric again appears. For the random structure, the majority of the faces have five edges, but a significant number have four and six edges, while for the symmetric structure, there are relatively few five-edged faces, and many more four- and six-edged faces. Indeed among all the symmetric-structure polyhedra, only 10% of the faces have five edges. This remarkable difference in the relative numbers of four, five and six edges clearly distinguishes random and symmetric structures. Once again we can say, given a single graph of the number of faces versus edges per face, for $N_v = 12$ to 16, i.e., given a single graph such as the ten shown in Fig. 10, we can positively identify the structure as random or symmetric.

In the random graphs in Fig. 10, there is a small but meaningful evolution as N_v increases. The number of six-edged faces is well below the number of five-edged faces at $N_v = 12$, but increases relatively as N_v increases, until the two are about the same at $N_v = 15$ and 16. In the symmetric graphs in Fig. 10, noteworthy evolution with increasing N_v is not apparent.

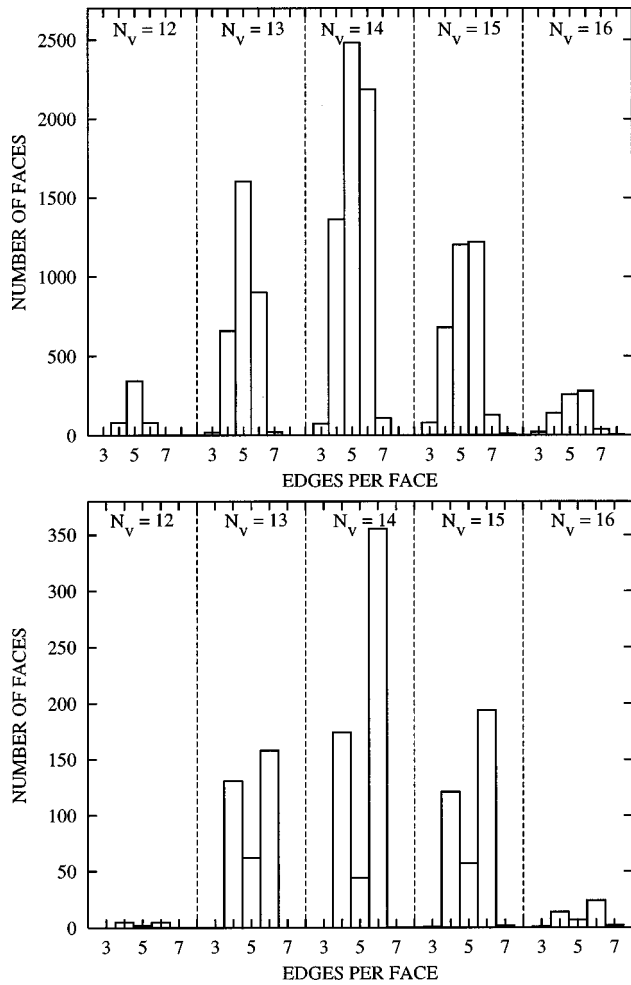


FIG. 10. Distribution of number of edges per Voronoi face for a random (top) and symmetric (bottom) structure. Both structures have $N=1000$. The random structure is at 0.0005 K and the symmetric one is at 0.013 05 K.

IV. COMPARISONS WITH EXPERIMENT

It has long been recognized that the split second maximum in $g(r)$ is an indication that a material may be amorphous. Extensive experimental work has been done to determine $g(r)$ for many different amorphous alloys and a lesser number of amorphous monatomic metals. The goal, in those earlier studies, was to uncover the underlying configurational order characteristic of amorphous materials. While these efforts are too many to review here, we will mention a sufficient number of them to obviate the relation between those efforts and the present theory.

We mention from the outset that we will not be concerned with amorphous alloys, but rather restrict ourselves to amorphous monatomic systems. The configurational order of the former requires investigating the partial pair distribution functions $g_{\alpha\beta}(|\mathbf{r}_\alpha - \mathbf{r}_\beta|)$ for species α and β (in a binary alloy g_{11} , g_{22} , and g_{12}). Since this case is beyond our present scope of interest, we make no mention of the relevance of our present work to alloys. Unfortunately, because of the relative ease of stabilizing amorphous alloys, many more experimental results exist for them than for amorphous monatomic systems.

The review of Angell [10] lists various experimental techniques used to structurally arrest materials in amorphous states. The experimental work discussed below relies on one such technique, namely, vapor deposition onto an ultracold substrate. In summary, these investigators (1) experimentally obtained supercooled states of various liquid metals (and alloys); (2) carried out scattering experiments using electron diffraction and then extracted the scattering intensity $I(k)$; and (3) having obtained an amorphous state, attempted to elucidate the underlying configurational order of the amorphous state by comparing the experimental $I(k)$, or its associated $g(r)$, to hypothesized theoretical models of amorphous materials. While the details of the experiments vary from investigator to investigator, the essence of each was to create thin films (20–1000 Å) by vapor deposition of the material onto either liquid-nitrogen or liquid-helium cooled substrates of various inert compositions. The experiments were done in ultrahigh vacuum (10^{-5} – 10^{-9} torr), and impurity contamination was extremely low. The rate of deposition was typically in the \AA s^{-1} range.

One of the earlier papers on this study was by Davies and Grundy [11]. Noncrystalline films of Ni, Co, and Co-P were obtained by vapor deposition of these materials onto liquid-nitrogen cooled collodion substrates. The films were generally metastable to crystallization and thus all configurational aspects of the study were performed *in situ*. The ambient pressure was 10^{-5} torr and the film thicknesses reached up to 1000 Å thick. Davies and Grundy then extracted $g(r)$ for these materials. Initial attempts to explain their experimental scattering functions in terms of fcc and hcp crystallites were unsuccessful. The authors also concluded that their experimental intensity curves could not be obtained by diffraction from small distorted fcc and hcp crystals arising from stacking faults. They also concluded that the packing was not consistent with models of dense random packing of hard spheres (DRPHS), though the agreement was better than for the microcrystalline models. We refer the reader to the review of Finney [12] for a discussion of DRPHS and its derivative models. What is of special interest to us is the $g(r)$ determined by Davies and Grundy as displayed in Fig. 2 of Ref. [11]. The split second maximum for both Ni and Co, characteristic of amorphous materials, has the same structure as we have found for supercooled Na. The intensity of the first subpeak of the split second maximum exceeds the intensity of the second subpeak. By immediate inspection, we expect that Davies and Grundy have arrested Ni and Co in the amorphous *random* state.

This work was soon followed by Ichikawa's [13] thin film studies on amorphous Ni and Fe, again by low-temperature condensation (liquid helium temperatures), in a high vacuum ($P=10^{-6}$ torr), in conjunction with an electron diffraction study. The substrate was polyvinyl formvar, film thickness reached 90 Å for Fe, and 20 Å for Ni, and the rate of deposition was 0.5 – 1.0 \AA s^{-1} . Many Ni films froze into fcc lattices when the film thickness was allowed to grow to 30 Å or more. Indeed, further work showed that increasing the impurity concentration in Ni facilitates the formation of the amorphous phase [14].

Upon analysis of the configurational order, Ichikawa concluded that Ni and Fe pack most consistently with dense random packing models [13]. Accordingly, he concluded that

these materials can not be described as an assemblage of minute crystals with bcc and fcc structure.

Of special interest to us is Fig. 4 in Ref. [13], which shows his Ni and Fe $g(r)$. Once again, these exhibit the same structure as we found for supercooled Na: the second maximum of $g(r)$ is split, and first subpeak exceeds the second subpeak.

The existence of an amorphous phase in Mn, Cr, plus Fe and Co films, was then proven by Leung and Wright [15]. We call to the readers attention, their experimental scattering functions, shown in Fig. 2 of Ref. [15], which again have the same split maximum structure as those of the previous two investigations. Failure to obtain agreement between experiment and microcrystalline models was extended by Leung and Wright to include fcc, strained and unstrained bcc, hcp with and without stacking faults, even also complex cubic structure A15. This finding was taken as evidence that the amorphous structure is a distinct phase and has no long-range order. It is interesting to note that Leung and Wright [15] also attempted to describe the underlying configurational order as being one that is seeded by both regular and irregular icosahedra; again these attempts were unsuccessful. This was also found to be the case by Wantanabe and Miida [16]. This finding is also consistent with the extensive recent work of LaViolette [6].

Leung and Wright [15] also summarize indirect evidence of a distinct amorphous phase. Their evidence includes resistivity, magnetoresistance, and magneto-optical measurements in Co; magnetization measurements in Fe; and Mossbauer hyperfine field and Hall measurements in amorphous cobalt.

Next we mention early MD calculations by Rahman, Mandell, and McTague [17] dealing with Lennard-Jones particles quenched to low temperatures (13 K for argon). They again found the split second maximum in $g(r)$ (Fig. 1, Ref. [17]) with the relative height of the first subpeak of the split second maximum being greater than the second subpeak. Once again, this is consistent with our picture that the system had been arrested in a *random* amorphous state. Rahman, Mandell, and McTague [17] noted the comparison of their $g(r)$ with models derived from DRPHS, but also rightfully point out the relevance of the soft-core portion of the potential. Further discussion into the importance of the soft core was given by Finney [12], who pointed out that the mediocre agreement achieved by using DRPHS could be improved by using random packing with more realistic potentials.

More recently, Ullo and Yip [18] carried out a detailed study of supercooled soft-sphere fluids using MD simulations. Their interest centered on uncovering a physical mechanism responsible for a theoretically proposed transition, distinct from the glass transition, predicted to occur in supercooled liquids. In the process of their study, Ullo and Yip calculated pair distribution functions for high densities. At a temperature corresponding to 72 K for argon, and densities approaching 0.7 of the hexagonal close-packing density, the second maximum on $g(r)$ split in a manner that is consistent with our universal $g_{\text{Ran}}(r)$, and characteristic of dense random packing. We expect qualitatively similar findings would hold for the density dependence of supercooled liquid sodium.

The experiments just reviewed leave little doubt that

many monatomic systems exist that can be arrested in an amorphous state characterized with pair distribution functions that closely match our $g_{\text{Ran}}(r)$ for supercooled Na. We believe that it is a small step to make the statement that these experiments have arrested the structure in *random* valleys. This view is supported by (1) the rapid cooling processes required to escape crystallization either in a perfect crystal or a microcrystalline state (our symmetric states); and (2) the extensive work done by these investigators indicating atomic random packing arrangements. Sodium, however, was obviously not in the list of elements that have been arrested in the random amorphous state. Insight into the reason for this is given by Angell, Clarke, and Woodcock [19], who examined the role of the interatomic potential in the formation of amorphous states. These authors assert that it is more difficult to amorphously arrest elements with softer cores (like the alkali metals with r^{-6}) than it is with elements with harder cores (like the transition metals with r^{-12}), because soft-core particles can move past each other more easily and thus find their way to the crystalline state. This simple picture is certainly consistent with known experimental results. While it is possible in our MD simulation to arrest the alkali metals, such as Na, in random valleys, quench times possible in the laboratory are far too long to escape crystallization.

V. CONCLUSIONS

Reference [7] considered energetics, stability, and kinetic properties of the random and symmetric states. Our purpose here was to investigate the atomic configurational order of these states. Omitting details, we summarize our most important conclusions as follows: (i) Both the pair distribution function and information on local positional order extracted from the Voronoi polyhedra support the hypothesis that random valleys have universal properties (in the limit of large N), consistent with the hypothesis of liquid-dynamics theory [1]. (ii) The symmetric valleys do not share these universal properties. (iii) Given a graph of $G_\gamma(r)$, one can positively identify its class as random, symmetric, or crystalline. (iv) Given a graph of the (1) distribution of Voronoi coordination numbers N_v , or (2) the angular distribution $P(\theta)$, for any N_v , or (3) the distribution of number of faces versus edges per face, as a function of N_v , we can positively identify the structure as random or symmetric. (v) For sodium the random pair distribution function has a split second maximum that is characteristic of many amorphous materials. We find that the first subpeak of the split maximum structure of Na exceeds the second subpeak. Experiments have shown this to also be the case for amorphous Ni, Co, Cr, Fe, and Mn. We believe that these experiments indicate that the random structure has been observed in the laboratory for the transition metals.

ACKNOWLEDGMENT

This work was supported in part by the U.S. Department of Energy under Contract No. W-7405-ENG-36.

- [1] D. C. Wallace, *Phys. Rev. E* **56**, 4179 (1997).
- [2] F. H. Stillinger and T. A. Weber, *Kinam* **3**, 159 (1981).
- [3] F. H. Stillinger and T. A. Weber, *Phys. Rev. A* **25**, 978 (1982).
- [4] T. A. Weber and F. H. Stillinger, *J. Chem. Phys.* **80**, 2742 (1984).
- [5] F. H. Stillinger and T. A. Weber, *Science* **225**, 983 (1984).
- [6] R. A. LaViolette and D. M. Stump, *Phys. Rev. B* **50**, 5988 (1994).
- [7] D. C. Wallace and B. E. Clements, preceding paper, *Phys. Rev. E* **59**, 2942 (1999).
- [8] A. C. Brown and R. D. Mountain, *J. Chem. Phys.* **80**, 1263 (1984).
- [9] C. E. Campbell, in *Progress in Liquid Physics*, edited by C. A. Croxton (Wiley, New York, 1978), p. 213.
- [10] C. A. Angell, *Science* **267**, 1924 (1995).
- [11] L. B. Davies and P. J. Grundy, *Phys. Status Solidi A* **8**, 189 (1971).
- [12] J. L. Finney, in *Amorphous Solids and the Liquid State*, edited by N. H. March, R. A. Street, and M. Tosi (Plenum, New York, 1985), p. 31.
- [13] T. Ichikawa, *Phys. Status Solidi A* **19**, 707 (1973).
- [14] M. R. Bennett and J. G. Wright, *Phys. Status Solidi A* **13**, 135 (1972).
- [15] P. K. Leung and J. G. Wright, *Philos. Mag.* **30**, 995 (1974).
- [16] D. Watanabe and R. Miida, *Jpn. J. Appl. Phys.* **11**, 296 (1972).
- [17] A. Rahman, M. J. Mandell, and J. P. McTague, *J. Chem. Phys.* **64**, 1564 (1976).
- [18] J. Ullo and S. Yip, *Phys. Rev. A* **39**, 5877 (1989).
- [19] C. A. Angell, J. H. R. Clarke, and L. V. Woodcock, in *Advances in Chemical Physics*, edited by I. Prigogine and I. A. Rice (Wiley Interscience, New York, 1981), Vol. 48, p. 397.